



**HAL**  
open science

# Equation of State and Structure of Electrostatic Colloidal Crystals: Osmotic Pressure and Scattering Study

V. Reus, L. Belloni, Thomas Zemb, N. Lutterbach, H. Versmold

► **To cite this version:**

V. Reus, L. Belloni, Thomas Zemb, N. Lutterbach, H. Versmold. Equation of State and Structure of Electrostatic Colloidal Crystals: Osmotic Pressure and Scattering Study. *Journal de Physique II*, 1997, 7 (4), pp.603-626. 10.1051/jp2:1997142 . jpa-00248466

**HAL Id: jpa-00248466**

**<https://hal.science/jpa-00248466>**

Submitted on 4 Feb 2008

**HAL** is a multi-disciplinary open access archive for the deposit and dissemination of scientific research documents, whether they are published or not. The documents may come from teaching and research institutions in France or abroad, or from public or private research centers.

L'archive ouverte pluridisciplinaire **HAL**, est destinée au dépôt et à la diffusion de documents scientifiques de niveau recherche, publiés ou non, émanant des établissements d'enseignement et de recherche français ou étrangers, des laboratoires publics ou privés.

## Equation of State and Structure of Electrostatic Colloidal Crystals: Osmotic Pressure and Scattering Study

V. Reus (<sup>1,\*</sup>), L. Belloni (<sup>1</sup>), T. Zemb (<sup>1</sup>), N. Lutterbach (<sup>2</sup>) and H. Versmold (<sup>2</sup>)

(<sup>1</sup>) CEA/Saclay, Service de Chimie Moléculaire, 91191 Gif-sur-Yvette Cedex, France

(<sup>2</sup>) Lehrstuhl für Physikalische Chemie II, RWTH Aachen, Templergraben 59, 52062 Aachen, Germany

(Received 2 September 1996, received in final form 13 December 1996, accepted 6 January 1997)

PACS.61.10.-i – X-ray diffraction and scattering

PACS.64.30.+t – Equations of state of specific substances

PACS.82.70.Dd – Colloids

**Abstract.** — Electrostatically stabilized aqueous suspensions of bromopolystyrene particles have been studied by scattering and osmotic pressure measurements. We investigated their structure and the interparticle interactions as a function of the volume fraction at very low salinity of the order of micromole/l. At slow crystallization speed we observe perfect crystals, body centered cubic crystals by light scattering for volume fractions between 0.04 and 0.7% and face centered cubic crystals by Ultra Small Angle X-ray Scattering (USAXS) for higher volume fractions (2–12%). After shear the crystal displays other structures. At low volume fractions (0.1–0.3%), some reflexions disappear by light scattering whereas a strong diffuse “prepeak” appears before the first Bragg peak for higher concentrations (2–12%) evidenced by USAXS. This “prepeak” can be attributed to defects in the crystal. Osmotic pressures have been measured by difference between the hydrostatic pressure in the solution and in the reservoir separated by an hemipermeable membrane. The experimental data are very well reproduced by the Poisson Boltzmann Cell (PBC) theory which shows that the interaction between particles is purely repulsive. No attractive contribution has been experimentally detected. By calculating the mean square displacement of a particle inside its cage from the eccentric PBC model, we have verified that the Lindemann criterion for the existence of crystals (against melting) is satisfied. This study has allowed to determine the equation of state of an electrostatic colloidal crystal and is equivalent to an ultraprecise force/distance measurement between latex particles since the measured forces are of the order of  $10^{-12}$  N for distances of the order of 4000 Å.

**Résumé.** — Des suspensions aqueuses de particules de bromopolystyrène ont été caractérisées par diffusion de lumière, diffusion de rayons X aux petits angles et par des mesures de pression osmotique. Nous avons ainsi étudié leur structure et les interactions interparticulaires en fonction de la fraction volumique à salinité constante de l'ordre de la micromole/l. Lorsque la cristallisation est lente, nous observons des cristaux parfaits cubiques centrés par diffusion de lumière pour des fractions volumiques comprises entre 0,04 et 0,7 % et cubiques faces centrées par diffusion de rayons X aux petits angles pour des fractions volumiques plus élevées (2–12 %). Après cisaillement, des défauts apparaissent dans les cristaux ; ils sont caractérisés par la disparition de certaines raies de Bragg en diffusion de lumière pour des échantillons de fraction volumique comprise entre 0,1 et 0,3 % et par la présence d'un pré-pic observé par diffusion de rayons X aux petits angles avant le premier pic de Bragg, pour des échantillons plus concentrés

---

(\*) Author for correspondence (e-mail: valerie@brownie.pc.rwth-aachen.de)

(2–12 %). Les pressions osmotiques ont été mesurées par différence de pression hydrostatique entre la solution et le réservoir séparés par une membrane hémiperméable. Les données expérimentales sont bien reproduites par la théorie Poisson Boltzmann Réseau (PBR) qui montre que les interactions sont purement répulsives. Aucune force attractive faible de longue portée n'a été détectée expérimentalement. En calculant le déplacement moyen d'une particule à l'intérieur de sa cage à l'aide du modèle PBR "excentré", nous avons vérifié que le critère de Lindemann était satisfait pour tous les cristaux observés. Cette étude a permis de déterminer l'équation d'état d'un cristal colloïdal électrostatique. Les résultats sont équivalents à une mesure de force ultraprécise puisque les forces d'interaction mesurées entre particules sont de l'ordre de  $10^{-12}$  N pour des distances centre à centre de l'ordre de 4000 Å.

## 1. Introduction

Like atomic crystals monodisperse colloidal suspensions can display a long range order. The typical size of latex colloidal particles is 100 to 1000 Å. Regular lattices can be observed in nature such as opals [1] or viruses [2–5]. Contrary to molecular crystals, it is easy to control interaction energy in colloidal crystals by means of the composition of the interparticle medium. Colloidal crystals have original properties intermediate between liquids and solids. Crystalline order requires a good monodispersity in size [6].

In the case of electrostatic colloidal crystals for which electrostatic repulsion is dominant, ionic strength of the solvent is the key parameter to modulate the long range interaction. These electrostatic colloidal crystals are already observed from less than 1%. In contrast hard sphere colloidal crystals appear above 49% [7].

The structure of synthetic latex colloidal crystals has been extensively studied, particularly by light scattering, for very low volume fractions [6,8]. We used a high resolution Bonse–Hart USAXS (Ultra Small Angle X–ray Scattering) camera to study samples in the concentration range 2–12%. Several groups [9–15] have determined the osmotic pressure by the osmotic compression method *i.e.* by dialysis against a calibrated stressor solution or with commercial osmometers for very concentrated samples (up to 60%) or for high ionic strength ( $> 10^{-6}$  M). It has been shown that measuring osmotic pressure in a crystal is equivalent to measuring a force between colloids. This has been introduced by Parsegian and coworkers [9] for lamellar liquid crystals of bilayers. Our aim is to extend these works to the regime of cubic colloidal crystals, focusing on the diluted part of the phase diagram in the absence of salt, where long range interaction dominate the system. Our final aim is to establish directly the pressure–distance relation for latex particles on the crystalline lattice, *i.e.* the equation of state.

In the present work, we report the use of a closed–loop deionization set–up which allows to combine the measurement of the osmotic pressure with scattering methods. It is thus possible to determine simultaneously the interaction forces and the structure. Osmotic pressures are measured by difference between the hydrostatic pressure in the solution and in the reservoir separated by an hemipermeable membrane. This approach has been pioneered by Ottewill *et al.* [16] for high concentrations. We explore the range of lower concentration (0.04–12%) at lower salinity (about  $10^{-6}$  M).

The existence of long range weak attractive interaction mechanism has been a debate for two decades. For instance, Ise *et al.* [17,18] have observed coexistence of pure liquid and colloidal crystals. Doshō and coworkers [19] have recently published a review of a large number of unexplained results in the literature aiming to this possibility. If a colloidal crystal coexists with a very diluted solution, the osmotic pressure stays constant but low at finite concentration.

This would be the first unambiguous proof of the existence of these forces and one of our objectives is to test for existence of these forces. The higher concentration regime for sterically ordered samples has been previously described by Bonnet-Gonnet *et al.* [10].

In this paper, we present results obtained by means of light scattering and ultra small angle X-ray scattering (USAXS) on highly charged colloidal crystals at rest and after shear induced by a peristaltic pump. Osmotic pressure measurements obtained with our closed set-up will be compared with theoretical models describing the interaction potential. Finally, the phase diagram of this system in diluted regime in the absence of salt will be established and discussed.

## 2. Experimental Section

### 2.1. MATERIAL

*2.1.1. Synthesis of Bromopolystyrene.* — In order to increase the electronic density contrast, we prepared bromopolystyrene particles by copolymerization in emulsion without surfactant. This type of synthesis has been previously described by Vanderhoff [20]. Parabromostyrene ( $C_8H_7Br$ , Fluka) is purified by distillation under reduced pressure in nitrogen before the copolymerization with sulfonate styrene ( $C_8H_7SO_3H = KVBS$ , Fluka). The initiator used is potassium persulfate ( $K_2S_2O_8$ ).

We fill a three-necked flask (2 l) with 700 ml of deionized water and stirred for 45 min under  $N_2$  to remove  $O_2$  to avoid a pre-initiation of the polymerization as well as an inhibition at the time of adding the monomers. This flask is immersed in a thermostat bath whose temperature is fixed to 82–83 °C. We add 34 g bromostyrene, 0.515 g KVBS and wait for thermal equilibrium. Then we incorporate into the solution 0.468 g  $K_2S_2O_8$ . Strong stirring is the key factor to obtain monodisperse particles. The latex is stirred with a magnetic stirrer. The polymerization lasts 24 hours under a weak stream of nitrogen. At the end of the polymerization, the solution is filtered to remove all aggregates. The weight fraction, determined by weighting a sample before and after drying in an oven at 80 °C, is about 4% in the reaction bath. The final pH of the reaction mixture is acid (pH  $\approx$  2) and the conductivity is high (130  $\mu S/cm$ ). Conductivity has to be reduced in order to avoid flocculation during the concentration of the solution. The solution is purified by dialysis in membrane bags (Visking 12–14 000 MW, Roth) which have been previously washed with deionized water. After several days, when the conductivity of the solution is a few  $\mu S/cm$ , we begin to concentrate the solution by osmotic stress with Dextran T110 as stressing polymer, or directly inside the closed set-up that we built and which is described below.

After washing the latex suspension, the ionic strength is  $\cong$  0.1  $\mu S/cm$ . The electrostatic repulsion between charged colloids is strong. Easily observable iridescence appears in the latex characteristic of the colloidal crystalline state. The distance between particles (comparable to the Debye length) is of the order of the wavelength of visible light. The iridescent coloration of the suspensions investigated in this study depends on the concentration: for our particles of diameter about 100 nm, the latex dispersion appears pink/green until a volume fraction about 5% with macroscopic crystallites visible with naked eyes, then becomes green/violet, violet/yellow. At about 7%, we see only diffuse colored bands because individual crystallites are so small that it is impossible to see them with naked eyes. Beyond 12% volume fraction, distances between particles correspond to ultraviolet wavelength. Therefore the sample appears milky similar to a sample unable to crystallize due to polydispersity. In this case, it is necessary to use the X-ray scattering to see if the sample is ordered or not. The size and shape of the crystallites have been studied by Okubo [21, 22] with silica and polystyrene particles. The nucleation and growth process, controlling the size of colloidal crystals have been described by

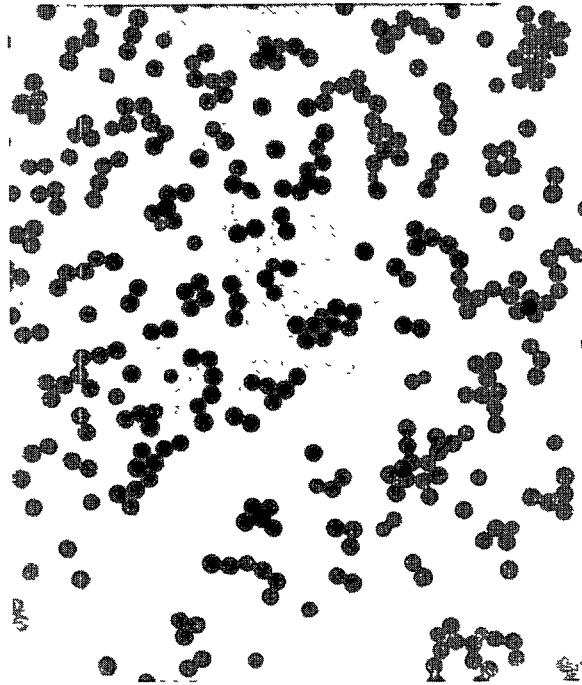


Fig. 1. — Transmission electron micrograph (TEM) of monodisperse bromopolystyrene spheres ( $\times 20\,000$ ). The radius of these particles is 50 nm.

Yoshida *et al.* [23]. In completely deionized and diluted suspensions it is possible to observe macroscopic crystallites of a few mm in size. The general tend is that the size of crystallites always decreases when the volume fraction  $\Phi_V$  increases.

We determined the density of these particles by densimetry as described in [24]; the density is  $1.565\text{ g/cm}^3$ . We use this value to convert the volume fraction from the weight fraction.

**2.1.2. Determination of the Radius  $a$ .** — As we can see from transmission electron microscopy (Fig. 1), the particles are spherical and monodisperse. The radius is about 50 nm. The hydrodynamic radius measured by quasielastic light scattering is 55 nm.

In the absence of interactions (dilute screened system,  $\Phi_V \approx 1\%$ ), the experimental X-ray scattering intensity  $I(q)$  (Fig. 2) can be assimilated to the form factor  $P(q)$  of the spherical particles:  $P(q) = \Phi_V \Delta\rho^2 f(qa)^2 V$  where  $V$  is the volume of one particle,  $\Delta\rho$  the electronic density contrast,  $\Phi_V$  the volume fraction and  $f(qa)$  the Bessel function of zero order:

$$f(qa) = 3 \frac{\sin(qa) - qa \cos(qa)}{(qa)^3}.$$

Such classical form factor presents a first zero minimum at  $qa = 4.5$  using the USAXS curve shown in Figure 2, one obtains  $a = 48\text{ nm}$  for our bromopolystyrene particles. If we try to fit the whole X-ray scattered intensity  $I(q)$  (knowing  $\Delta\rho$  and  $\Phi_V$ ) with the average radius  $a$  as the fitting parameter, one obtains  $a = 51\text{ nm}$  (see Fig. 2). These four results obtained for the radius as determined by transmission electron microscopy, quasielastic light scattering, minimum of form factor and fitting of X-ray scattering intensity  $I(q)$  are consistent within 10%, showing that particle distribution is essentially monodisperse to 10% precision.

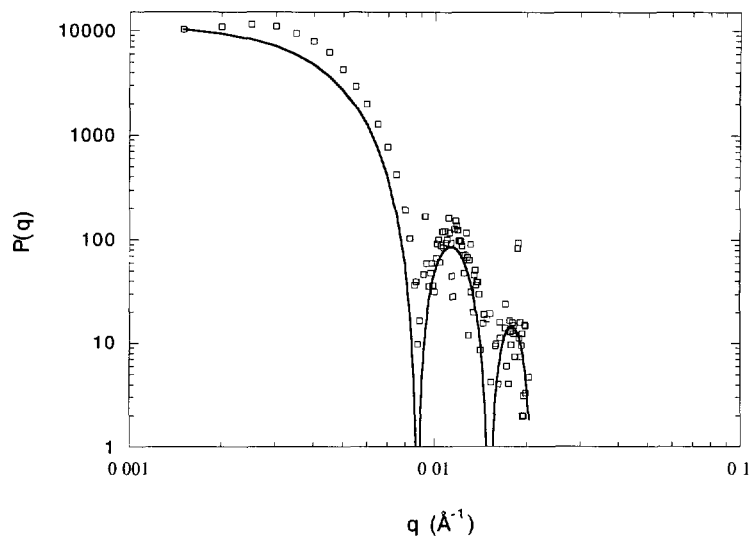


Fig. 2. — Experimental (squares) and theoretical (solid line) form factor  $P(q)$  in log-log scale for a sample with a volume fraction equal to 0.1% containing  $10^{-4}$  M of NaCl. The theoretical form factor is obtained for a sphere of radius 51 nm and an electronic density contrast equal to  $4.54 \times 10^{10}$  cm $^{-2}$

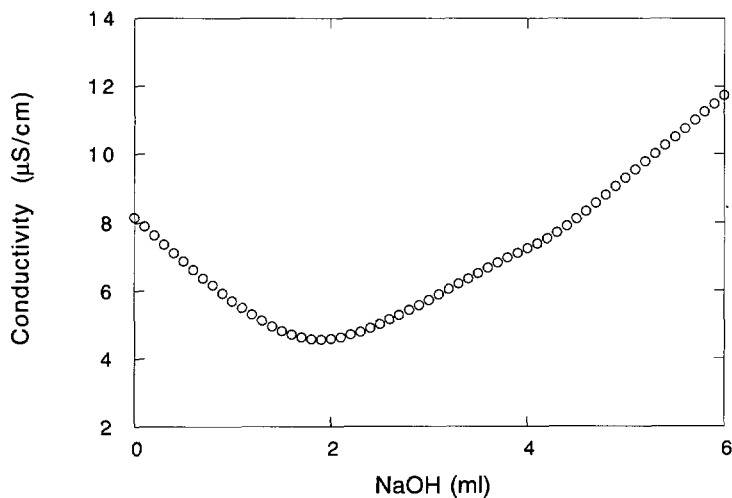
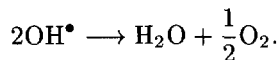


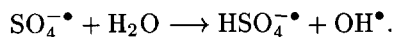
Fig. 3. — Conductimetric titration of a diluted latex suspension (0.13% volume fraction) without added salt; measurement of the conductivity of the solution in  $\mu\text{S}/\text{cm}$  versus added  $10^{-3}$  M NaOH.

*2.1.3. Determination of the Number of Ionizable Sites.* — The stability of the dispersion is due to the presence of ionic groups at the surface of particles which come, for the most of them, from radicals formed by the decomposition of the initiator and sulfonated styrene. The number of ionizable sites has been assessed by a conductimetric titration (Fig. 3) as described in [24]. 50 ml of dialyzed latex of concentration  $3 \times 10^{18}$  part/m $^3$  or 0.13% in volume fraction (determined by light scattering on the crystallized solution) were titrated against  $10^{-3}$  M

NaOH at 25 °C. A continuous stream of N<sub>2</sub> eliminated the atmospheric CO<sub>2</sub>. Two points of equivalence are observable in the titration curve: the first corresponds to the number of strong acid groups at the surface of one particle (sulfate and sulfonate surface groups, 7100 acid groups), and the second to the number of weak acid groups (10 600 groups). These are probably carboxylate surface groups (pK<sub>a</sub> ≈ 4.2) due to the oxidation of hydroxyl groups, which can occur even under nitrogen atmosphere due to the reaction:



Thus, it is possible to have some oxygen in the solution. OH groups can be formed by the hydrolysis of sulfonated groups on the surface through the Kolthoff reaction [25,26]:



The initiator (S<sub>2</sub>O<sub>8</sub><sup>2-</sup>) decomposes itself to give SO<sub>4</sub><sup>•-</sup> which lead by hydrolysis to hydroxyl groups.

In these oxidation conditions occurring during the polymerization, hydroxyl groups of the surface can be oxidized in carboxyl groups:



Thus, a total number 17 700 ionizable sites corresponding to a maximum charge of 0.54 electron/nm<sup>2</sup> are potentially ionizable at the surface of a particle. Knowing the pH of the solution, the structural charge equal to the number of ionized sites, is weaker than the total number of ionizable sites. It depends on the concentration but is of the order of 7500 or 0.2 electron/nm<sup>2</sup>.

## 2.2. METHODS

*2.2.1. Measurement of the Osmotic Pressure.* — We built an experimental set-up designed to measure the difference in hydrostatic pressure (water level) between the solution and a reservoir separated by a dialysis membrane (Fig. 4). This set-up allows to control different intensive parameters as the ionic strength *I*, which is the most important parameters to obtain electrostatic colloidal crystals, or the pH-value. It is composed of two circuits, the reservoir containing the solvent (and salt) and the solution containing the particles, the counter-ions (and salt). The two circuits are in contact in a cell, made of two Plexiglas plates (130 mm diameter), separated in two parts by an ultrafiltration membrane (Millipore, 0.025 μm pore size). This filter allows ions and solvent exchanges between the two circuits but prevents the particles of crossing through the membrane. The Plexiglass plates are grooved in 2 mm thickness along a "spiral" to force the solution to circulate everywhere in the cell in following this "spiral" way. This method ensures to obtain a homogeneous concentration in the sample volume. "Tygon" tubing link this cell to the other elements of the circuits. The conductivity (C) and the pH in the two circuits are permanently controlled with a conductimeter (WTW) and a pH-meter (Jenco). The presence of ionic exchange resins (R) (Fluka Amberlyst 15 and A27) in the reservoir and the solution allows to eliminate all ionic impurities and to keep the ionic strength down to micromoles when needed. A loss of latex due to its adsorption on the ionic exchange resins cannot be avoided. Therefore the latex volume fraction is determined after each scattering measurement. Two vertical quartz tubes (1 mm diameter and 30 cm height) open on the top to the air, are branched to the circuits very near the cell. At equilibrium, the difference Δ*h* of levels between the two tubes gives the osmotic pressure Π through the

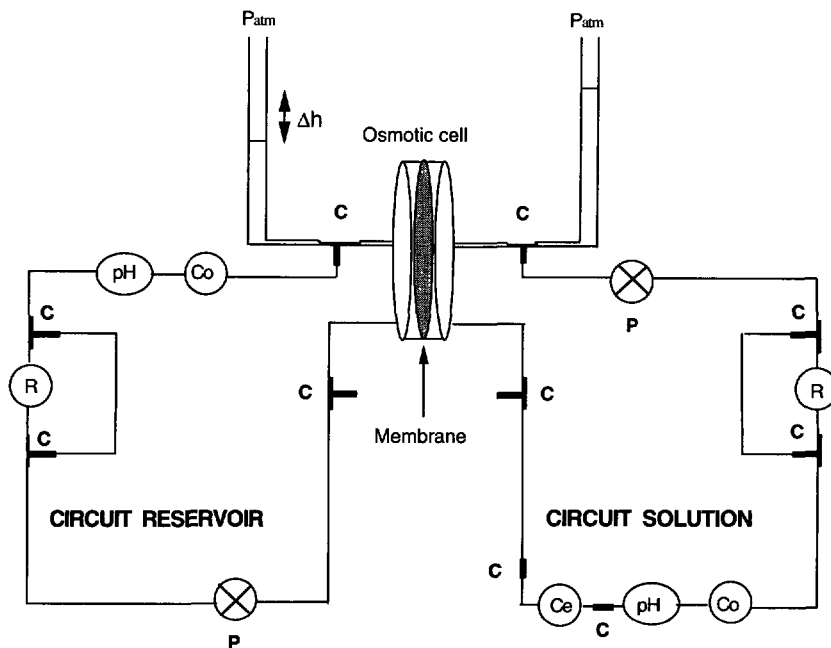


Fig. 4. — Experimental set-up used to measure the osmotic pressure and determine the structure of colloidal crystals simultaneously. (R) ion exchange resin, (Co), (pH) and (Ce), measuring cells (conductivity, pH and scattering), (P) peristaltic pump, (C) teflon cocks.

hydrostatic law  $\Pi = \rho g \Delta h$  ( $\rho$  is the density of water,  $g$  the gravity acceleration). We previously used the same experimental arrangement to measure the osmotic pressure of liquid suspensions containing polydisperse particles which could not crystallize [24]. In the present work we study crystallized suspensions in a wider concentration range; these two factors contribute to the increasing of viscosity of the samples and equilibrium times. For this reason, some improvements have been introduced in the apparatus in order to reduce the equilibration times. First we decided to reduce the overall volume of the circuit. Then, the quartz tubes are located as close as possible from the membrane. We added three ways cocks (C) at the exit of the cell in the two circuits to disconnect the cell and tubes from the rest of the circuit during the equilibration of the water levels.

The experimental procedure is as follows: first, we filled the two circuits with deionized water and pumped with two peristaltic pumps (P) during a few hours to eliminate all ionic impurities. When the conductivity is about  $0.1 \mu\text{S}/\text{cm}$ , we stopped the circulation. Then we verified that the levels in the two tubes were the same (zero osmotic pressure). We replaced water with about 50 ml latex solution in one of the two circuits. We pumped again in the two circuits to eliminate impurities. At equilibrium, we measured the water levels in the two tubes by using a cathetometer. The water level differences typically were from one millimeter to a few centimeters. The incertitude on the measurement was about one millimeter or  $\pm 15 \text{ Pa}$ . Errors due to differences of interfacial tension and density between the latex and the solvent were negligible.

In order to reduce the time needed for obtaining the value of an osmotic pressure and to improve the precision of the water level data, we used the dynamic method described by Fuoss and Mead [27]. This method is based on the measurement at different times of the water

height difference  $\Delta h$  between the two parts of the closed circuit. It consists to determine the asymptote of the curve  $(\Delta h) = f(t)$  (pressure *versus* time). First the levels in tubes are imposed such that  $\Delta h$  is 1 or 2 cm *above* the estimated final equilibrium value  $\Delta h_{\text{eq}}$ ; when the two menisci move respectively down and up, the measurement of the height difference between the levels of the two compartments is made every 30 s during 8 to 10 minutes. After this typical time the menisci move more and more slowly and many hours or days would be necessary to reach the asymptotic value. Then the same operation is carried out starting with  $\Delta h$  levels 1 to 2 cm *below* the estimated final equilibrium value. The arithmetic sum (half-sum) of the two measurements, at equal intervals, is plotted against time. This value reaches the equilibrium value much more rapidly and gives the osmotic pressure of the solution after just a few minutes.

Because of the viscosity of the sample it was necessary to stir the latex between two consecutive measurements. A vibrating plate was placed against the cell and tubes to accelerate equilibrium. After 1–2 minutes we stopped the vibration and waited for a few minutes, which is the time needed to reach the local equilibrium in the vicinity of the membrane; then we noted down the  $\Delta h$  values. We started again to agitate for a few minutes and determined the new  $\Delta h$  values until we obtained the true equilibrium which is reached when the concentration in the cell and in the tubes is homogeneous. We worked in this way in the two directions from height differences higher and smaller than the presumed value. Thanks to this method, we considerably reduced error bars and obtained two points per day in concentrated range ( $> 4\%$ ) and three or four for more diluted samples.

A quartz capillary or a cell (Ce) were inserted in the latex circuit to determine simultaneously the structure of the sample by X-ray or light scattering, respectively. The cylindrical quartz cell used for light scattering had a diameter of 0.8 cm and a height of about 5 cm; the rounded quartz capillary was 1 mm in diameter and open-ended.

**2.2.2. Scattering Apparatus.** — Light scattering experiments have been performed with (a) a correlation spectrometer with photomultiplier [28] and with (b) a multichannel spectrometer with CCD-camera [29]. Light sources were respectively a helium–neon (632.8 nm) and an argon (532 nm) laser.

The small angle X-ray apparatus is a Bonse–Hart camera [30] which has been built in our laboratory and is described elsewhere [31, 32]. All scattering curves have been deasmeared to the method proposed by Strobl [33]. The resolution was of the order of  $3 \times 10^{-4} \text{ \AA}^{-1}$ . The vertical resolution of the Bonse–Hart machine was set to  $7 \times 10^{-2} \text{ \AA}^{-1}$  *i.e.* 200 times the horizontal plane resolution.  $q$  range of USAXS measurement was from  $q_{\text{min}} = 5 \times 10^{-4}$  to  $q_{\text{max}} = 10^{-2} \text{ \AA}^{-1}$  for a typical countage time of 4 h with a 8 kW source.

### 3. Results and Discussion

**3.1. SCATTERING RESULTS.** — For extremely low volume fractions ( $0.04 < \phi_V < 0.3\%$  in our case), colloidal crystals can be studied by light scattering. Multiple scattering is negligible and peaks are in the correct scattering vector  $q$  range for light scattering ( $q_{\text{min}} = 1.1 \times 10^{-4}$  to  $q_{\text{max}} = 3.2 \times 10^{-3} \text{ \AA}^{-1}$ ) in that concentration range. In this case, one observes perfect crystals: the peak at lowest  $q$  is the first Bragg peak ( $q_B$ ) and no diffuse peak is observed.

Perfect crystals without diffuse peak have also been observed with USAXS in the range  $2 < \phi_V < 12\%$  without added salt for samples in sealed capillaries (1 mm diameter) containing ionic exchange resins. The dispersion has been injected in the capillary using a syringe and was kept at rest for a few hours. Optical microscopy has shown that samples are polycrystalline; they appear as a “powder” of small randomly oriented crystallites.

The scattering intensities are plotted in reduced units,  $q_n/q_B$ . One obtains results as shown in Figure 5a for light scattering and 5b for USAXS. Indexing for bcc and fcc is indicated. The large number of Bragg peaks allows unambiguously the identification of a bcc packing at low concentration turning towards fcc packing at high volume fractions as expected and already observed by Sirota *et al.* [34] and Monovoukas and Gast [35].

Diluted samples (0.1 to 0.3% in volume fraction) have been studied in a quartz glass cell of 0.8 cm in diameter. After shearing they presented coloured bands on the cell walls, which could be interpreted as a hexagonal structure of uncorrelated layers. As one can see in Figure 6a definite crystallites at the bottom of the cell can be seen as well. We determined the structure of these samples by light scattering at different heights in the cell and found always at the bottom a perfect bcc equilibrium structure. This can be seen in Figure 6b, where the first five bcc peaks are identified definitely. In the same figure one can see a scattering curve measured for the "layered" structure: here the second and fifth peaks are missing and the peak relations in  $q$  are  $\sqrt{1}:\sqrt{3}:\sqrt{4}$ . This is expected for a two-dimensional hexagonal structure. Such structures have been theoretically described [36] and observed under shear [37–39] and at rest [38, 39]. Particles can form independently layers which are oriented by shearing and slide over each other. After stopping the shear the structure corresponding to the equilibrium structure is not observed on the time scale of the experiment but laterally uncorrelated layers remain frozen in a layer structure.

Nevertheless, one might expect a peak shift, if the internal crystalline structure of the same latex sample changes from one packing into another [40, 41]. Such a peak displacement cannot be observed in our case.

There are many points which confirm our conclusion of a hexagonal layer structure. Experimental results were absolutely reproducible with any sample and with any optical set-up. Quartz cells were rotated during scattering experiment permanently to avoid any loss of peaks. The above mentioned "coloured-bands-structure" occurred at the beginning of crystallization and was only observable directly on the cell walls [41]. Besides this structure is stable even under shearing in the closed circuits.

We turn now towards the more concentrated regime measurable with USAXS ( $2 < \phi_V < 12\%$ ).

Consider a colloidal crystal of volume fraction  $\Phi_V = 3.5\%$ . The USAXS curve obtained during circulation of the latex sol in the set-up previously described is shown as a solid line in Figure 7. The dashed line corresponds to the USAXS curve measured when the fluid is at rest in the capillary. The circulation of the dispersion in a quartz capillary of a diameter of 1 mm and a flow rate of the order of 0.1 ml/s induces enough shear to melt the crystal into a sol. This experiment underlines one of the characteristics of colloidal crystals; they are destroyed by stirring due to the weak value of their elastic modulus (between 0.1 and 1000 dyn/cm<sup>2</sup>). The size of one colloidal particle is about 1000 times higher than that of an atom and the density of the system is  $10^{12}$  times weaker explaining the high elasticity of the colloidal crystals [42, 43]. The peak  $B_1$  ( $q = q_B$ ) observed in these two experiments corresponds to the average distance between repulsive particles and is not very different in the liquid and crystalline states. The strong peak  $D_1$  appearing at lower  $q$  ( $q = q_D$ ) at rest does not correspond to this distance. This observation demonstrates that the origin of this peak cannot be the distance between the nearest neighbours because it would correspond to a hypothetical volume fraction  $\Phi_V^{\text{hyp}} = 0.85\%$  for a fcc crystal, instead of the known value of  $\Phi_V = 3.5\%$ .

As mentioned in the introduction we could be in the presence of a microphase separation between a colloidal crystal and large holes filled with a sol of concentration close to  $\Phi_V^{\text{hyp}}$ , as suggested by Ise and coworkers [17–19]. However, this explanation is incoherent with measured osmotic pressures as well as the observation of a constant ratio between the positions of the

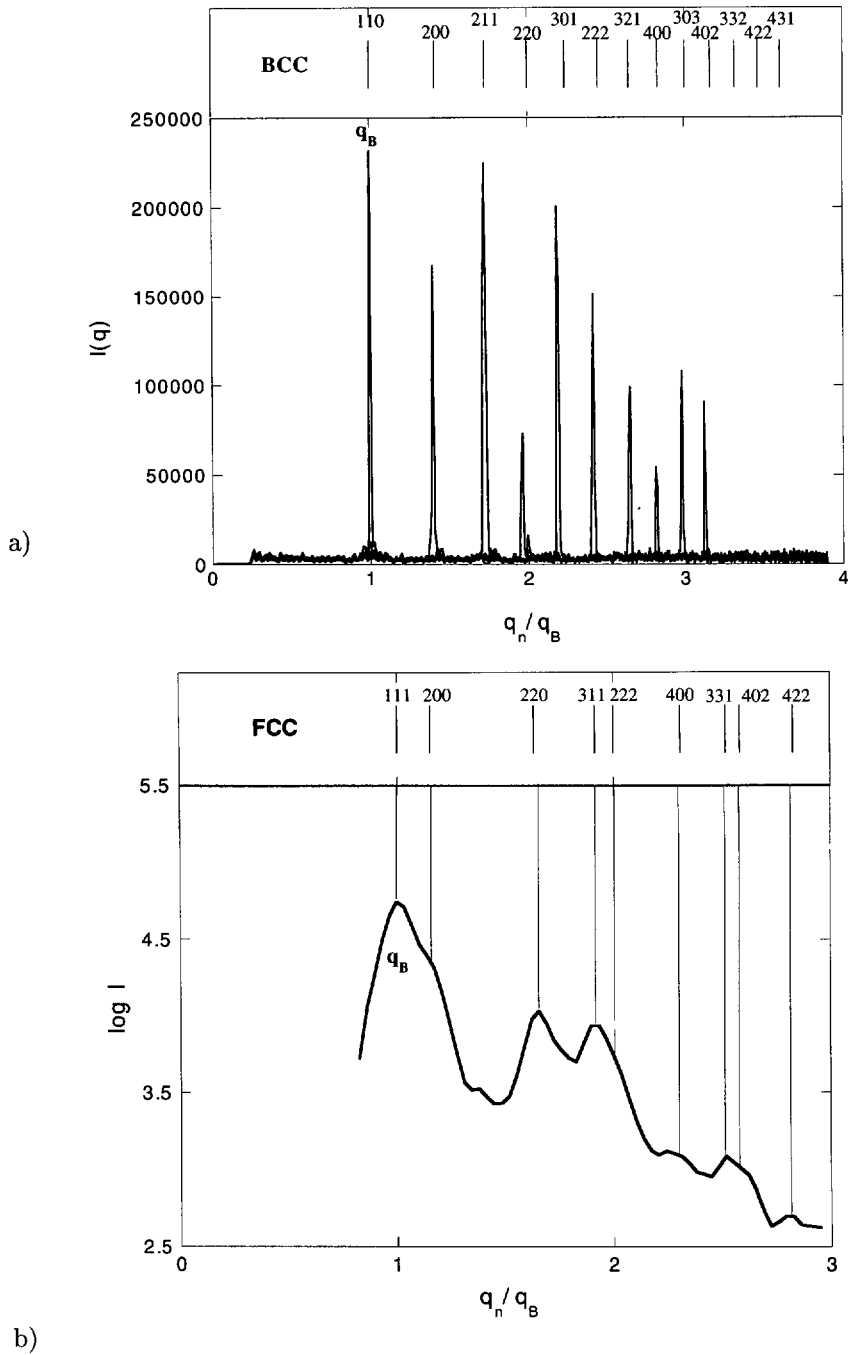


Fig. 5. — a) Light scattering result ( $\lambda = 532$  nm, multichannel photometer) of a sample with a volume fraction of 0.07% in reduced units  $q_n/q_B$ .  $q_n$  is the position of the  $n^{\text{th}}$  Bragg peak, and  $q_B = q_1$ . Peak positions corresponding to a bcc structure are indicated. b) Small Angle X-ray scattering (USAXS) curve of a sample with a volume fraction of 4% in reduced units  $q_n/q_B$ . Peak positions corresponding to a fcc structure are indicated.

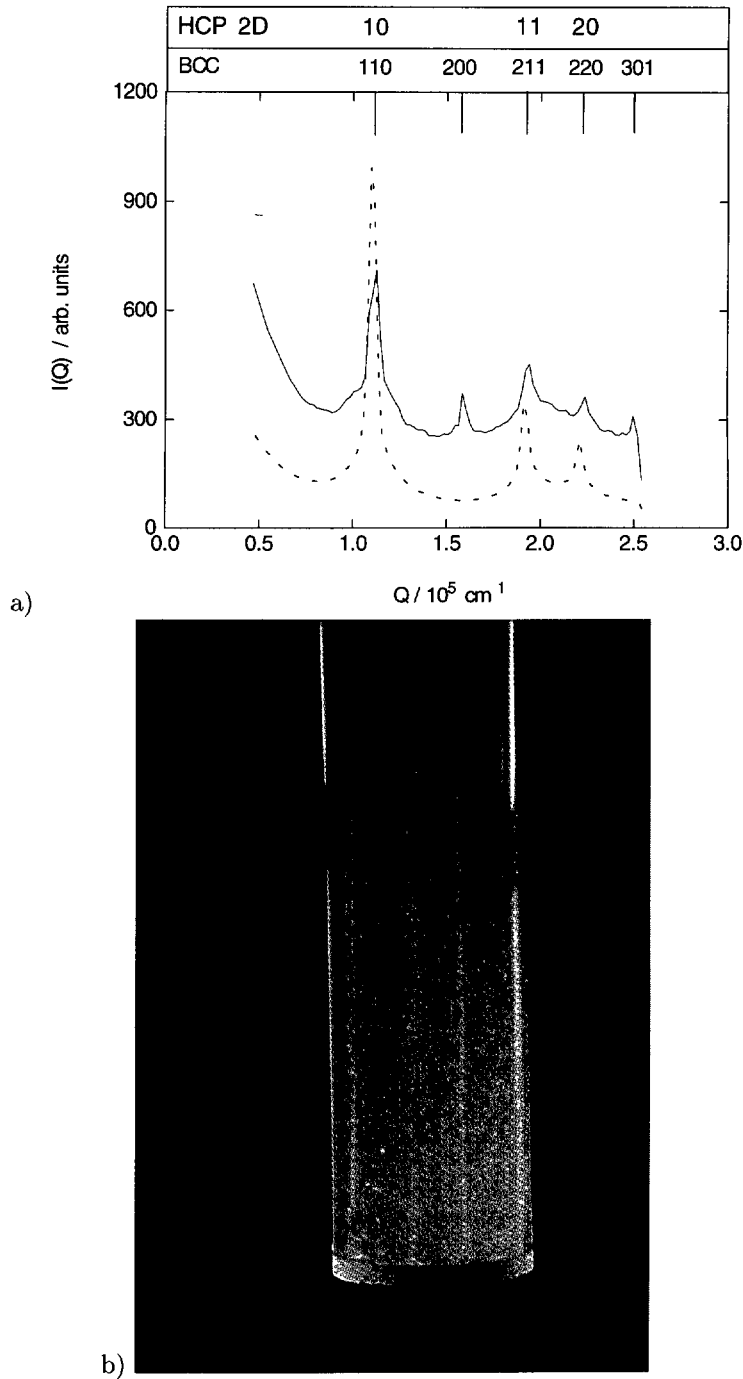


Fig. 6. — a) Light scattering curve ( $\lambda = 632.8$  nm) of a sample with a volume fraction 0.2%. The solid line corresponds to the scattering of the sample containing crystallites in the bottom of the cell (bcc structure). The dashed line represents the scattering of perceptibly layers in the upper part of the cell. b) Photography of a diluted colloidal crystal. In the lower part, one observes crystallites (bcc structure) while in the upper part layers appear characteristic of non equilibrium structure.

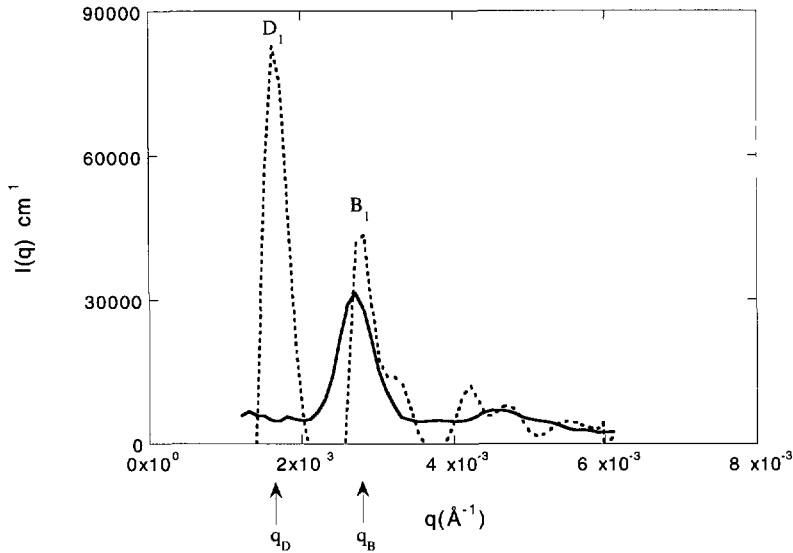


Fig. 7. — Small angle X-ray scattering (USAXS) deasmeared curves of a deionized sample with a volume fraction equal to 3.5% placed in the set-up described; at rest (dashed line) and under shear (full line).

first peak observed at  $q = q_D$  and the second peak obtained at rest at  $q = q_B$ . Figure 8 shows the positions of these two peaks *versus*  $\Phi_V^{1/3}$ . Any microphase separation between two compositions such as a crystal and a diluted sol would produce constant positions for  $q_D$  and  $q_B$  together with different relative intensities. We observe a constant ratio  $q_D/q_B = 0.66$ . The first peak observed for the crystal at rest cannot be the first Bragg peak: its origin has to be related to defects producing diffuse scattering inside the first cell in reciprocal space. A similar observation of a strong diffuse peak has been reported by Pusey outside the first lattice cell [44].

For volume fractions between 2 and 12% the diffuse peak  $D_1$  located at  $q = q_D$  is always obtained for samples in the closed circuit. A coexistence between two types of cubic crystals (bcc and fcc) could explain these observations. The samples at volume fractions between 2 and 8% are drawn in arbitrary units in Figure 9. A systematic trend towards broadening of Bragg peaks related to smaller size of crystallites limits the number of observed peaks when volume fraction increases above 8%. We recorded the intensity of a sample in the circuit after 6, 8, and 10 days. We notice that the diffuse scattering peak corresponding to the presence of defects does not disappear. The crystal has not enough time to reorganize itself in a few days. Particles are frozen or their movements are very slow; a reorganization would need maybe a few months or years.

The strong diffuse peak  $D_1$  observed with USAXS is always observed at  $q_D/q_B = 0.66$ . Stacking faults have already been observed in colloidal crystals. For instance, opals can be arranged in random hexagonal layers hcp ( $\beta = 0.5$ ) where  $\beta$  is the defect parameter. A coexistence between fcc and hcp with defect domains has been already observed [45]. Pusey *et al.* [44] observed by light diffraction a 3D hcp structure with growth defects. Laun *et al.* [46] investigated the behaviour of concentrated dispersions electrostatically stabilized in ethylene glycol under shearing by Small Angle Neutron Scattering (SANS). The intensity profiles  $I(L)$  along these Bragg rods give an information on the stacking order. Versmold [47] gave an

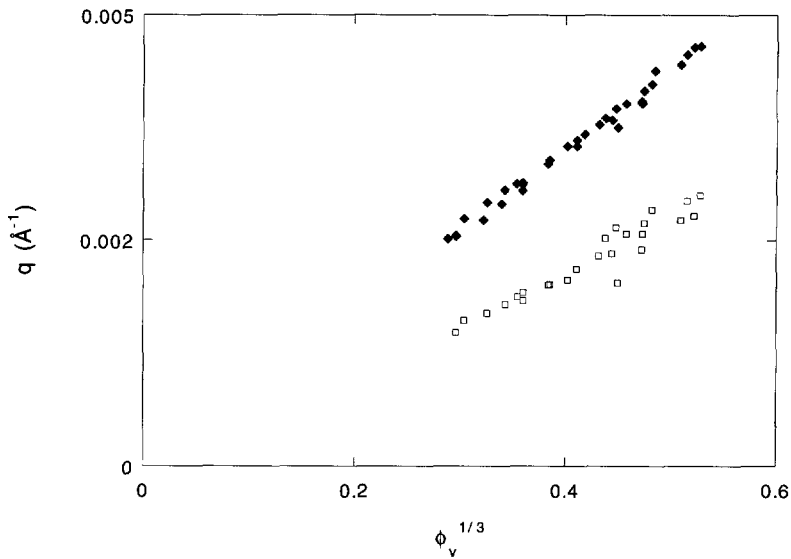


Fig. 8. — Scattering vector  $q = q_D$  in  $\text{\AA}^{-1}$  of the first peak (open squares) and  $q = q_B$  the second peak (filled squares) observed at rest versus  $\Phi_V^{1/3}$

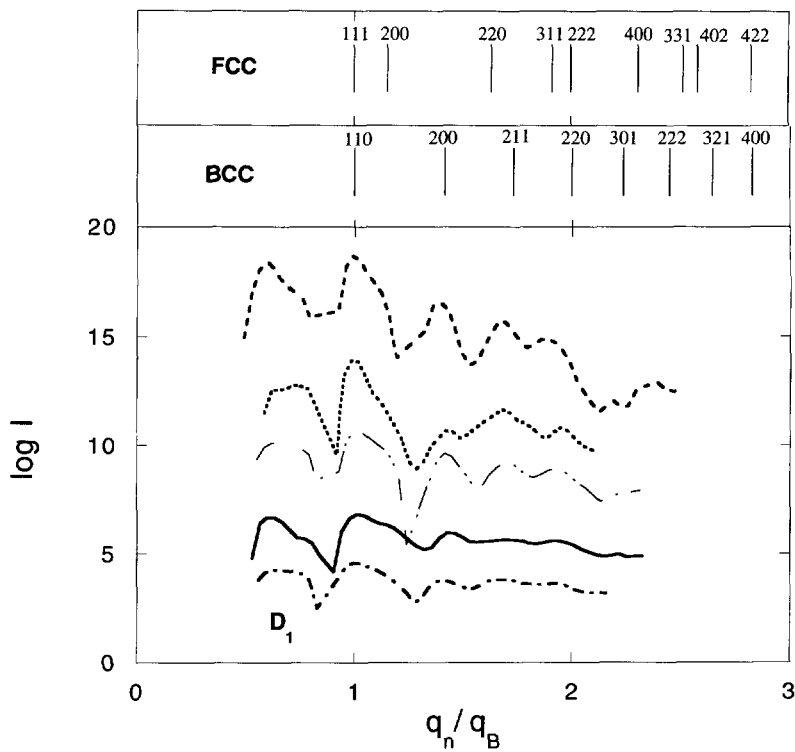


Fig. 9. — Small angle X-ray scattering (USAXS) curves for different volume fractions 2% (---), 3.5% (- - - -), 5.5% (- - - -) and 8% (—) are represented in reduced units  $q_n/q_B$ . Peak positions corresponding to a crystal with defects are indicated.

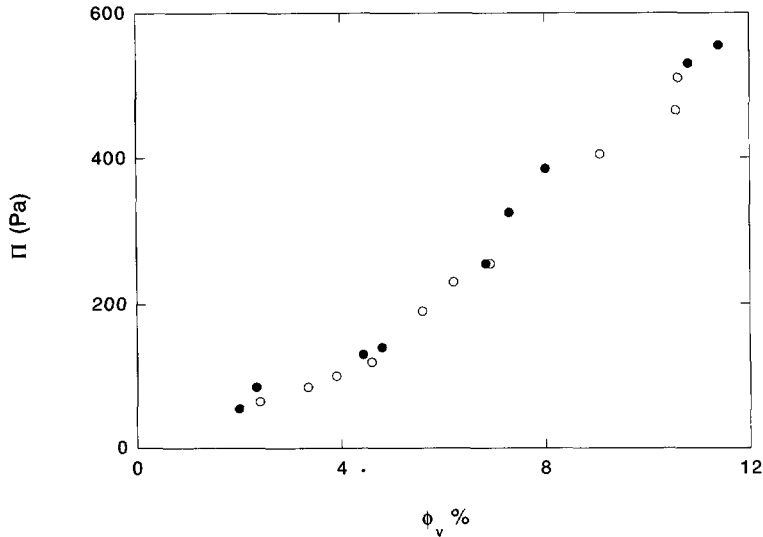


Fig. 10. — Variation of the experimentally measured osmotic pressure  $\Pi$  of bromopolystyrene dispersions (in Pascal) at a salinity  $10^{-6}$  M in the reservoir as a function of the volume fraction. The open circles are obtained during dilution while filled circles are obtained during concentration of the sample.

explanation to this observation. But stacking faults always produce diffuse scattering at higher  $q$  than the first Bragg peak [48], while we observed it always at lower  $q$  values. At the present stage, the origin of this peak inside the first lattice cell can only be attributed to defects in the crystal. This peak is however surprisingly sharp and strong which means that some correlation between defects must occur.

Defects as missing latex particles in the lattice due to insufficient diffusion during crystallite growth process can be proposed to explain the presence of this diffuse peak. Its position would be then related to an average distance between holes which is higher than the lattice constant of the crystal [49].

We have no experimental proof of that mechanism. Further work is in progress to clarify this point and to attribute the origin of the diffuse peak.

In summary, depending of the concentration, the following structures have been identified: at rest without shear, perfect bcc and perfect fcc. In the range of 2–12% in volume fraction (after turning the circulation off) a fcc structure with strong diffuse peak for  $q_D/q_B = 0.66$  and some possible fcc/bcc coexistence in the same sample are observed.

**3.2. OSMOTIC PRESSURE RESULTS.** — First, we measured the osmotic pressure for a latex suspension of 2% volume fraction with the set-up previously described. Then we concentrated the sample step by step *in situ* until 12% and measured the pressure for each concentration. These data correspond to the filled points shown in Figure 10. To verify that the compression is reversible, we diluted the sample in the circuit with deionized water to come back from 12% to 2% and obtained the data points shown as open circles. Pressure increases monotonically with concentration. No plateau or hysteresis is observed. Samples are always monophasic.

At all concentrations ( $2 < \Phi_V < 12\%$ ) a finite non zero value of the osmotic pressure has been measured: the possibility of holes in equilibrium with a colloidal crystal as often reported in literature [17–19] is undoubtedly excluded by our experiments.

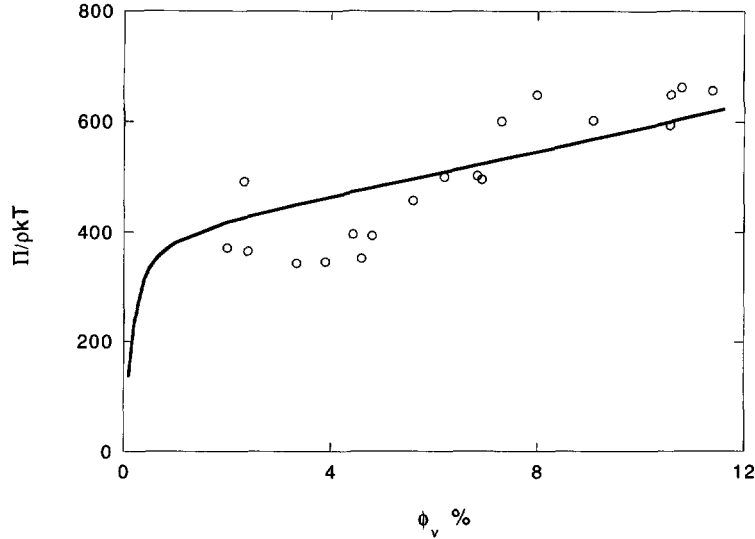


Fig. 11. — Experimental  $\Pi/\rho kT$  (open circles) are compared to the theoretical  $\Pi/\rho kT$  (solid line) calculated with the Poisson Boltzmann Cell (PBC) model for a salinity in the reservoir equal to  $10^{-6}$  M and a particle radius of 510 Å.

We plotted the data in reduced units  $\Pi/\rho kT$  versus the volume fraction  $\Phi_V$  in Figure 11 where  $\rho$  is the number concentration of the colloids. The value of  $\Pi/\rho kT$  is nearly constant ( $\approx 500$ ) in the volume fraction regime 2–12% and lies between the value 1 for perfect gas pressure of colloid particles alone and the value  $Z^{\text{str}}$  for perfect gas pressure of all counterions. This can be understood as the number of “free”, uncondensed counterions per colloid or as the effective colloidal charge. Note that this notion of effective charge is introduced just for an illustration and is not of absolute necessity at this point.

We used the classical Poisson Boltzmann Cell (PBC) theory to calculate the osmotic pressure of these solutions: the solution is divided in spherical, globally neutral, cells of radius  $R$ . A colloidal particle is located at the center of each cell. The volume fraction  $\Phi_V = (a/R)^3$  determines the radius of the cell. The ionic profiles  $c_{\pm}(r)$  of the monovalent counter-ions and co-ions calculated between the surface of the particle and the surface of the cell  $a < r < R$  are related to the reduced electrostatic potential  $\varphi(r) = \frac{e\Psi(r)}{kT}$  by  $c_{\pm}(r) = c'_S \exp(\pm\varphi(r))$  where  $c'_S$  is the salinity in the reservoir. These two relations implicitly assume that  $\varphi = 0$  in the reservoir and state the equality of the chemical potential of the salt in the solution and in the reservoir (Boltzmann approximation).

$\varphi(r)$  is deduced from the Poisson-Boltzmann equation

$$\Delta\varphi(r) = \varphi'' + \frac{2}{r}\varphi' = \kappa'^2 \text{sh}(\varphi(r))$$

with the boundary conditions (constant charge assumption)

$$\frac{d\varphi}{dr}(a) = -\frac{Z^{\text{str}}L_B}{a^2}; \quad \frac{d\varphi}{dr}(R) = 0$$

$Z^{\text{str}}$  is the structural colloidal charge (number of ionized sites),  $L_B = \frac{e^2}{4\pi\epsilon_0\epsilon kT}$  is the Bjerrum length and  $\kappa' = (8\pi L_B c'_S)^{1/2}$  the Debye screening constant in the reservoir.

Note that when the salinity in the reservoir  $c'_S$  tends to zero, the potential  $\varphi(r)$  diverges as  $-\ln c'_S$ , the co-ion concentration vanishes and the counterion profile becomes independent of the value of  $c'_S$ , as expected.

The Poisson Boltzmann equation is solved numerically by iterations [50]. After numerical resolution the osmotic pressure  $\Pi$  is determined from the total ionic concentration at the edge of the cell [51, 52]:

$$\Pi = kT(c_+(R) + c_-(R) - 2c'_S) = 4kTc'_S \text{sh}^2 \left( \frac{\varphi(R)}{2} \right).$$

As usual for highly charged colloids, what happens “far” from the particle near the edge of the cell and thus osmotic pressures are independent of  $Z^{\text{str}}$

We calculated the osmotic pressure with PBC model and noticed that our experimental data are in agreement with these calculations. The Poisson Boltzmann Cell (PBC) [10, 51, 52] model allows to predict the pressure knowing only the salt concentration in the reservoir evaluated by conductimetry and the radius previously determined equal to 510 Å. The theoretical curve  $\Pi/\rho kT = f(\Phi_V)$  calculated by the PBC model decreases very quickly below 1% and it is nearly constant in the region 2–12% and reproduce very well the experimental data. Here again, the existence of any weak long range attractive interaction is excluded. This is due to the finite, non zero, salt concentration in the reservoir ( $10^{-6}$  M). At zero volume fraction  $\Pi/\rho kT$  reaches the value 1 as expected for a very dilute colloidal solution in presence of salt (in absence of salt, the asymptotical value of  $\Pi/\rho kT$  at zero volume fraction would be  $Z^{\text{str}}$ ). It is important to note that there is no need for any attractive intervention to interpret our results, even at vanishing concentration.

Another theoretical approach which can be investigated to calculate the osmotic pressure is the so-called One Component Model (OCM). The starting point of this approach which considers explicitly only the colloids is an effective, in-averaged, colloid-colloid potential. We take the simple, screened-Coulombic, DLVO expression:

$$\beta V(r) = \frac{Z_{\text{eff}}^2 L_B}{r} \frac{\exp(-\kappa(r - 2a))}{(1 + \kappa a)^2}$$

$Z_{\text{eff}}$  is here an effective charge which is introduced to correct in some artificial way the linearized Debye Hückel colloid-ion approximation implicitly assumed in the DLVO expression. In our highly charged systems  $Z_{\text{eff}}$  is much lower than  $Z_{\text{str}}$ .  $\kappa(\text{Å}^{-1}) = 0.33\sqrt{I(\text{mol/l})}$  depends on the ionic strength  $I$  of the solution, sum of the salt and the free counterions contribution  $I = \frac{Z_{\text{eff}}\rho}{2} + c_S$ .

Using the classical statistical mechanics theory of liquids based on the Ornstein-Zernike (OZ) equation and the HNC integral equation [53], we have calculated the pair distribution function  $g(r)$  from the potential  $V(r)$ . Lastly, the osmotic pressure has been deduced from the virial equation:

$$\frac{\beta\Pi}{\rho} \approx 1 - \frac{\rho}{6} \int_0^\infty r g(r) \frac{d\beta V(r)}{dr} 4\pi r^2 dr.$$

Note that, due to the strong repulsion between the colloids,  $g(r)$  presents a high and narrow first peak located at the mean distance between neighbours  $r = d_V$  if one approximates this peak by a delta function (of same integral), the virial equation becomes:

$$\Pi \approx \rho kT + \frac{\rho}{6} F(d_V) N_V d_V \approx \frac{F(d_V)}{(\sqrt{2}/4)d_V^2} \quad (1)$$

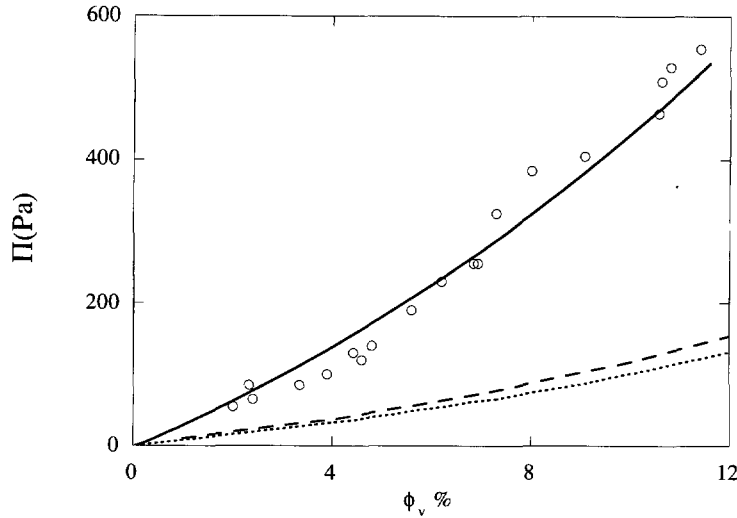


Fig. 12. — Experimental osmotic pressure results (open circles) are compared with the PBC model (solid line) and the One Component Model (dashed lines): (---) HNC + virial equation, (- - - -)  $g(r) \approx \delta$  function + virial equation (relation (1)).

where  $N_V$  is the number of nearest neighbours,  $d_V$  the distance between nearest neighbours, equal to  $d/\sqrt{2}$  where  $d$  is the lattice constant for a fcc cell  $F(d_V) = -\frac{dV(d_V)}{dr}$  and the DLVO force between them.

Taking a fixed effective charge  $Z_{\text{eff}}$  equal to 700 in agreement with those used for the phase diagram which we'll discuss below, one obtains pressures which are lower than measured pressures and the PBC pressures as shown Figure 12. This is because only a part of the interaction is included in this way. A similar effect has been observed in concentrated sol [10] and in diluted suspensions with polydisperse particles [24]. This reflects the fact that the pressure is essentially due to the counterions. Since the OCM does not take them explicitly into account, it intrinsically fails to correctly reproduce the osmotic pressure. Note in Figure 12 that the relation (1) is a good approximation of the virial pressure.

It is possible to relate the osmotic pressure  $\Pi$  to a force  $F$  between particle  $F = \frac{\Pi S}{N_V}$ . The unit Wigner-Seitz cell associated to the fcc crystal is a regular rhombic dodecahedra with  $N_V = 12$  square faces. The total surface  $S$  can be assimilated to a sphere of radius  $d_V/2$ . Since the osmotic equilibrium experiments consist in compressing the Wigner-Seitz cell, the observed pressure is the pressure calculated from the excess ion concentration at the edge of the Wigner cell modelled theoretically by a sphere. Difference between sphere and dodecahedra is not experimentally measurable. The measurable force by our technique is about  $10^{-12}$  N (shown in Fig. 13) which is very weak compared to the performances of the force balances developed in the ten last years.

#### 4. Comparison with Theoretical Phase Diagrams

Many theoretical phase diagrams of charged colloidal systems have been established [55–58]. For highly charged systems the colloidal particles adopt spontaneously a 3D ordered structure

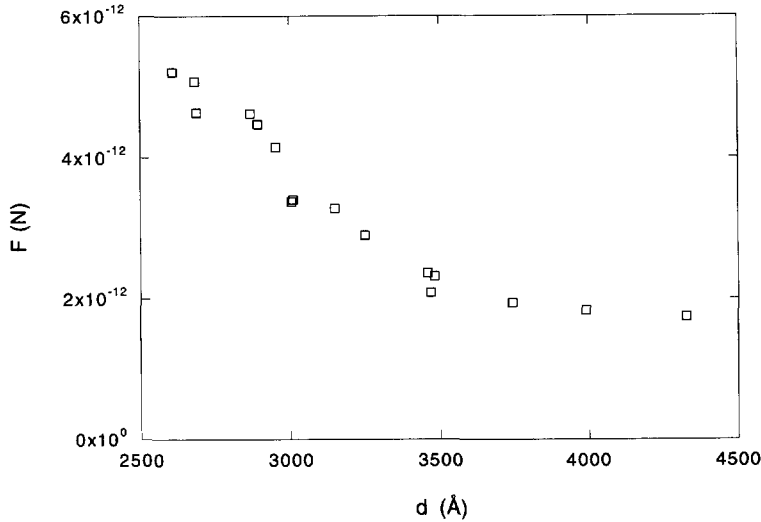


Fig. 13. — Force in Newton obtained by dividing the measured osmotic pressure by the surface of a sphere (radius  $d_V/2$  where  $d_V$  is the distance between the nearest neighbours) and the number of nearest neighbours  $N_V$  versus lattice constant  $d$ .

to minimize the repulsive interparticle interaction energy. The structure of the crystal is determined by parameters as the concentration of particles, the effective charge, the ionic strength of the solution and the diameter of the particles. Statistical mechanics simulation show universal behaviour according to the two reduced variables.

Robbins *et al.* [55] have established a phase diagram  $kT/U(d_V)$  as a function of  $\lambda$  by molecular dynamic simulations (MD).  $\lambda$  represents the number of Debye length  $\kappa^{-1}$  existing between two neighbour particles in the lattice ( $\lambda = \kappa d_V$ ) where  $d_V$  is the mean distance between two particles.  $kT/U(d_V)$  represents the “stiffness” of the colloidal crystal in reduced units. They used a Yukawa potential for point like charged particles:

$$\frac{kT}{U(d_V)} = \frac{d_V}{Z_{\text{eff}}^2 L_B \exp(-\kappa d_V)}$$

We compared our data to those predicted from theoretical results obtained by Robbins *et al.* Remember that our diluted samples have a bcc structure which has been determined by light scattering and are represented by open circles in Figure 14. More concentrated samples have a fcc structure observed by X-ray scattering (full circles). In Figure 14, the top of the figure is a soft dispersion while the bottom is a stiff solution. Note that going from the most diluted sample to the most concentrated, the crystal first broadens and then softens under the effect of his own counter-ions.

We have located our charged system in this diagram with one adjustable parameter which is the effective charge. Our experimental results are in agreement with those founded by Robbins *et al.* using the Alexander effective charge [59] or a fixed charge equal to 700 to calculate the potential.

As it can be seen in Figure 14:

- i) the transition from bcc to fcc is at the expected location;

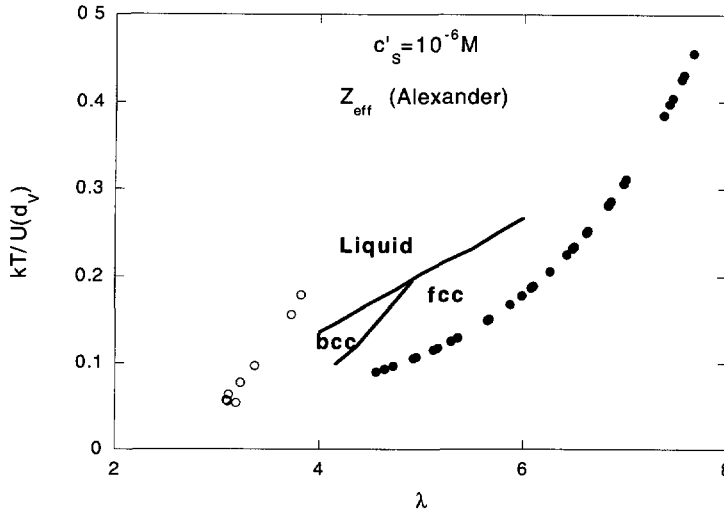


Fig. 14. — Phase diagram  $kT/U(d_V)$  versus  $\lambda = \kappa d_V$ . Filled circles are obtained from our X-ray data (fcc structure) and open circles from our light scattering results (bcc structure) of bromopolystyrene dispersions. Salinity in the reservoir is  $10^{-6}$  M. The Alexander effective charge was used to calculate the potential  $U(d_V)$ . Comparison is made to the calculations of reference [55] using molecular dynamics (solid lines).

- ii) a crystal is obtained in a region where a liquid is expected: the solid is slightly “stiffer” than predicted by the model. If one takes in account the finite size of the particles in the Yukawa potential, a better agreement may be obtained.

Lindemann [60] proposed a useful and very general empirical criterion for predicting the liquid–crystal transition which states that a crystal melts when  $\alpha = \langle u^2 \rangle^{1/2} / d_V \geq 0.1$ .  $\alpha$  is the ratio of the mean square displacement of a particle around its equilibrium position in the crystal divided by the size of its cage (or the distance  $d_V$  between neighbours). In the following, we will use the eccentric PBC model to calculate  $\langle u^2 \rangle^{1/2}$  and to test the validity of Lindemann criterion [61].

In the usual PBC configuration the colloid is located at the center of the spherical cell and feels no force. In order to be able to evaluate the mean square displacement, it is necessary to know the price to pay to shift the colloidal particle away from its equilibrium position. In the eccentric spherical cell model, the colloid is centered at the position  $\mathbf{u}$  relative to the center of the cell. By axial symmetry, the force  $\mathbf{F}$  felt by the particle is opposite to  $\mathbf{u}$  and, for small displacement  $u$  (harmonic approximation) and can be expressed as  $\mathbf{F} = -k\mathbf{u}$  where  $k$  is a spring constant. The particle moves inside a potential well of the form  $U(\mathbf{u}) = U_0 + 1/2ku^2$ .  $\langle \mathbf{u} \rangle = 0$  by symmetry while  $\langle u^2 \rangle$  can be obtained from:

$$\langle u^2 \rangle = \frac{\int_0^\infty e^{-\beta U(u)} u^4 du}{\int_0^\infty e^{-\beta U(u)} u^2 du} = \frac{3}{\beta k}$$

Note that the precise value of the upper limit in the integrals of the equation above is not important and can be taken as infinite.

In the Appendix the eccentric PBC model is solved in the limit of small eccentricity. The spring constant  $k$  is obtained as a simple integral of the classical (centered) PBC solution  $\varphi_0(r)$

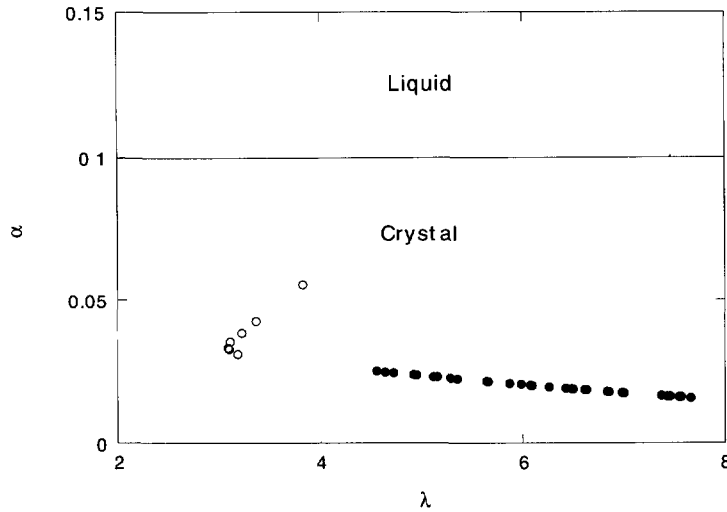


Fig. 15. — Lindemann parameter  $\alpha$  (see text) calculated in the PB eccentric model for our data as a function of  $\lambda = kd_V$ . The critical value for melting is  $\alpha_c \cong 0.1$ .

(see Eq. (A.7)). This leads for  $\langle u^2 \rangle$  to:

$$\langle u^2 \rangle = 9L_B \int_a^R \frac{2 + \kappa'^2 s^2 \text{ch} \varphi_0(s)}{s^4 \varphi_0'^2(s)} ds. \quad (2)$$

Then, the Lindemann parameter is given by  $\alpha = \frac{\sqrt{\langle u^2 \rangle}}{2R}$ .

This approach has the advantage not to use the effective charge. In Figure 15 we plotted this parameter as a function of  $\lambda$  for a constant salinity in the reservoir equal to  $10^{-6}$  M. Only the volume fraction varies. If one considers that the crystal melts when  $\alpha$  is higher than 0.1 (criterion valid for molecular crystals), our experimental points correspond to a crystalline phase whatever the volume fraction. The parameter increases for weak volume fractions since particles have a bigger freedom in movement. On the other hand we have not any informations about the structure of the crystal. We find here that Lindemann criterion is always valid, since the structure is crystalline and the average distance from equilibrium position for a given particle is always less than 10% of the lattice constant.

## Conclusion

In the absence of salt, the electrostatic colloidal crystals that we have studied in diluted regime are dominated by repulsive electrostatic interaction. Knowing the osmotic pressure and the structure of the crystal, we established the pressure–distance relation *i.e.* the equation of state and its phase diagram at a constant salinity.

At larger distances than the nearest neighbour distances we observed by USAXS a strong diffuse band. The history of the sample strongly influences the presence of this diffuse peak. We observed a perfect fcc structure during a slow crystallization. Under shear by a peristaltic pump the crystallization is very quick and particles have no time to organize themselves perfectly; one observes (in this case) a diffuse peak related to the presence of defects in the crystal. This peak is situated before the first Bragg peak and is likely due to the presence of holes

in the crystal. The reorganization is extremely slow, it does not occur at the time scale of one week.

After shear for very diluted samples layers appear. These samples have been studied by light scattering. Some Bragg peaks are missing. That could be interpreted as a 2D hexagonal layer structure.

With a precision of millimeter water level pressure purely electrostatic interaction is the dominant term in all our samples. We translated these pressures in forces between particles. Order of magnitude is about  $10^{-12}$  N.

Our osmotic pressure measurement technique is equivalent to a very precise force apparatus for large distances. This property may be used to investigate the effect of adding mono and multivalent salt on our colloidal system to modulate the interparticle interaction.

## Acknowledgments

This work has been realized thanks to Procope program n° 94222 between the RWTH (Aachen, Germany) and CEA (Saclay, France). We thank Jacques Lambard for his help in performing USAXS experiments and the Institut für Kunststoff-Verarbeitung for his help in performing TEM photos. We thank Prof Strobl for making available to us the commented source code of his program.

## Appendix

### Eccentric Poisson-Boltzmann-Cell Model

The spherical colloid is now centered at the position  $\mathbf{u} = u\mathbf{z}$  with respect to the center of the spherical cell (kept as the origin of the coordinates). By axial symmetry a point inside the cell is characterized by the spherical coordinates  $r$  and  $\theta$ , where  $\theta$  is the angle between  $\mathbf{r}$  and  $\mathbf{u}$  (see Fig. 16). In the following we will assume that the shift  $u$  is small and expand all quantities up to the first order in  $u$ . This linear expansion is sufficient to deduce the spring constant  $k$ . For example, the reduced electrostatic potential is expressed as:

$$\varphi(r, \theta) = \varphi_0(r) + \varphi_1(r) \cos \theta$$

where  $\varphi_0(r)$  is the solution of the spherically symmetric PB equation previously calculated. The function  $\varphi_1$  is proportional to  $u$ .

The full solution  $\varphi(r, \theta)$  must verify the non spherically symmetric PB equation  $\Delta\varphi = \kappa'^2 \text{sh}\varphi$ . Expanding  $\text{sh}\varphi$  up to first order leads to the following linear differential equation for the function  $\varphi_1(r)$ :

$$\varphi_1'' + \frac{2}{r}\varphi_1' - \frac{2}{r^2}\varphi_1 - \kappa'^2 \text{ch}(\varphi_0)\varphi_1 = 0. \quad (\text{A.1})$$

The symbols ' and '' represent the first and second derivatives.

The boundary condition at the edge of the cell ( $r = R$ ) is simply  $\varphi_1'(R) = 0$  (Gauss's law for the neutral cell). That at the colloidal surface ( $r = a + u \cos \theta$ ) is deduced from the Gauss's law, already satisfied by  $\varphi_0$ , which relates the normal electric field to the colloidal charge (constant charge assumption):

$$\varphi_1'(a) = -u\varphi_0''(a).$$

Equation (A.1) verified by  $\varphi_0$  can be integrated in first time to give:

$$r^2(\varphi_0'\varphi_1' - \varphi_0''\varphi_1) = C. \quad (\text{A.2})$$

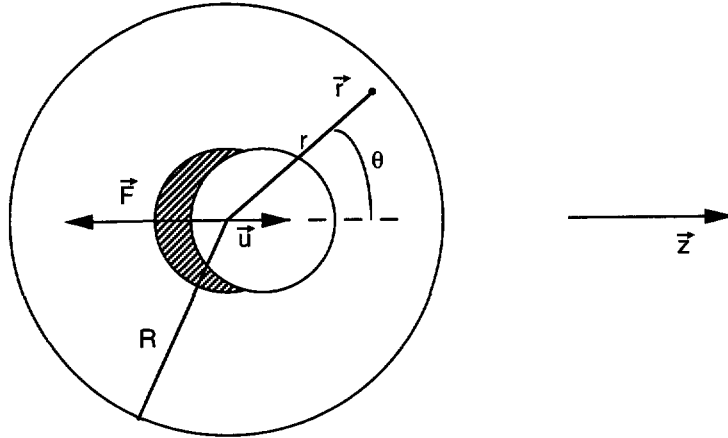


Fig. 16. — Eccentric PB cell geometry.

As it is shown below the constant  $C$  is directly related to the force experienced by the colloid. Indeed, in the PB approximation this force is obtained by integrating the Maxwell tensor  $\mathbf{T} = \mathbf{T}_{el} + \mathbf{T}_{th}$  on any closed surface containing the particle inside (since  $\text{div } \mathbf{T} = 0$ ).

$$T = \varepsilon_0 \varepsilon \left( \frac{kT}{e} \right)^2 \left( \nabla \varphi \cdot \nabla \varphi - \frac{1}{2} \nabla \varphi^2 I \right) - kT c_{ion} I. \quad (\text{A.3})$$

Choosing as closed surface the surface of the sphere of radius  $r$ , the force  $\mathbf{F}$ , obviously aligned with  $\mathbf{u}$ , becomes:

$$F = \int \int_r (\mathbf{T} \cdot d\mathbf{S})_z = \frac{kT}{3L_B} r^2 (\varphi'_0 \varphi'_1 - \varphi''_0 \varphi_1). \quad (\text{A.4})$$

Thus, the first primitive (A.2) just expresses that the calculation of  $F$  is independent of the choice of the integration surface. Moreover,  $C = 3L_B \beta F$ . Equation (A.2) can be integrated another time to give:

$$\varphi_1(r) = \varphi'_0(r) \left[ C' + C \int_a^r \frac{ds}{s^2 \varphi_0''(s)} \right]. \quad (\text{A.5})$$

The constants  $C$  and  $C'$  will be obtained from the two boundary conditions. Some precaution must be taken in using equation (A.5) at  $r = R$  since  $\varphi'_0(R) = 0$  and the integral diverges. Starting from the PB equation verified by  $\varphi_0$  an integration by part of the integral allows to eliminate this problem:

$$\int_a^r \frac{ds}{s^2 \varphi_0''(s)} = \left[ \frac{1}{s^2 \varphi_0''(s) \varphi_0'(s)} \right]_a^r - \int_a^r \frac{2 + \kappa'^2 s^2 \text{ch} \varphi_0(s)}{s^4 \varphi_0''^2(s)} ds. \quad (\text{A.6})$$

Then the two boundary conditions on  $r = a$  and  $r = R$  can be directly applied to give the two integration constants and consequently the force  $F$  applied on the colloid and the spring constant  $k = -F/u$ :

$$k = \left( 3\beta L_B \int_a^R \frac{2 + \kappa'^2 s^2 \text{ch} \varphi_0(s)}{s^4 \varphi_0''^2(s)} ds \right)^{-1} \quad (\text{A.7})$$

Equation (2) for the mean square displacement  $\langle u^2 \rangle$  follows from equation (A.7).

This powerful eccentric PBC approach allows to calculate non spherically symmetric properties without solving anything but the usual spherical PB equation.

## References

- [1] Sanders J.V., *Nature* **204** (1964) 1151.
- [2] Stanley W.M., *Science* **81** (1935) 644.
- [3] Bernal J.D. and Fankuchen I., *J. Gen. Physiol.* **25** (1941) 111.
- [4] Williams R.C. and Smith K.M., *Nature* **179** (1957) 119–120.
- [5] Klug A., Franklin R.E. and Humphreys–Owen S.P.F., *Biochim. Biophys. Acta* **32** (1959) 203–219.
- [6] Pusey P.N., in “Liquids, Freezing and Glass Transition”, Les Houches Session LI, D. Levesque, J.P. Hansen and J. Zinn–Justin, Eds. (Elsevier, Amsterdam, 1991).
- [7] Pusey P.N. and Van Megen W., *Nature* **320** (1986) 340.
- [8] Härtl W. and Versmold H., *J. Chem. Phys* **88** (1988) 11.
- [9] Parsegian V.A., Fuller N. and Rand R.P., *Proc. Natl. Acad. Sci* **76** (1979) 2750.
- [10] Bonnet–Gonnet C., Belloni L. and Cabane B., *Langmuir* **10** (1994) 4012–4021.
- [11] Rohrsetzer S., Kovacs P. and Nagy M., *Colloid Polym. Sci.* **264** (1986) 812–816.
- [12] Barclay L., Harrington A. and Ottewill R.H., *Kolloid Z. Z. Polym.* **250** (1972) 655–666.
- [13] Homola A. and Robertson A.A., *J. Coll. Interface Sci.* **54** (1976) 286–297.
- [14] Dickinson E. and Patel A., *Coll. Polym. Sci.* **257** (1979) 431–433.
- [15] Goodwin J.W., Hearn J., Ho C.C. and Ottewill R.H., *Br. Polym. J.* **5** (1973) 347–362.
- [16] Goodwin J.W., Ottewill R.H. and Parentlich A., *Colloid Sci.* **268** (1990) 1131–1140.
- [17] Ise N., Okubo T., Sugimura M., Ito K. and Nolte H.J., *J. Chem. Phys.* **78** (1983) 1.
- [18] Ise N. and Matsuoka H., *Macromolecules* **27** (1994) 5218–5219.
- [19] Dosho S., Ise N., Ito K., Iwai S., Kitano H., Matsuoka H., Nakamura H., Okumura H., Ono T., Sogami I.S., Ueno Y., Yoshida H. and Yoshiyama T., *Langmuir* **9** (1993) 394–411.
- [20] Vanderhoff J.W., *J. Colloid Interface Sci.* **28** (1968) 336–337.
- [21] Okubo T., *Colloid Polym. Sci.* **271** (1993) 190–196.
- [22] Okubo T., *Langmuir* **10** (1994) 1695–1702.
- [23] Yoshida H., Ito K. and Ise N., *J. Chem. Soc. Faraday. Trans* **87** (1991) 371–378.
- [24] Reus V., Belloni L., Zemb T., Lutterbach N. and Versmold H., *J. Chim. Phys.* **92** (1995) 1233–1256.
- [25] Stone–Masui J. and Watillon A., *J. Colloid Interface Sci.* **52** (1975) 479–503.
- [26] Dunn A.S. and Chong L.C., *Sym. J.* **2** (1970) 49.
- [27] Fuoss R.M. and Mead D.J., *J. Phys. Chem.* **47** (1943) 59.
- [28] Härtl W., Versmold H. and Wittig U., *Langmuir* **8** (1992) 2885.
- [29] Härtl W., Klemp R. and Versmold H., *Phase Transitions* **21** (1990) 229–242.
- [30] Bonse U. and Hart M., *Appl. Phys. Lett.* **7** (1965) 238–240.
- [31] Lambard J., Lesieur P. and Zemb Th., *J. Phys. I France* **2** (1992) 1191–1213.
- [32] Lesieur P., Lindner P., Desforge C., Lambard J. and Zemb Th., *Physica B* **180&181** (1992) 564–566.
- [33] Strobl G.R., *Acta Cryst. A* **26** (1970) 367.
- [34] Sirota E.B., Ou–Yang H.D., Sinha S.K., Chaikin P.M., Axe J.D. and Fujii Y., *Phys. Rev. Lett.* **62** (1989) 1524–1527.
- [35] Monovoukas Y. and Gast A., *J. Colloid Interface Sci.* **128** (1989) 533–548.

- [36] Brindley G.W. and Méring J., *Acta Cryst.* **4** (1951) 441–446.
- [37] Ackerson B.J. and Clark N.A., *Phys. Rev. Lett.* **46** (1981) 2.
- [38] Ashdown S., Markovic I., Ottewill R.H., Lindner P., Oberthür R.C. and Rennie A.R., *Langmuir* **6** (1990) 303–307.
- [39] Versmold H. and Lindner P., *Langmuir* **10** (1994) 3043–3045.
- [40] Dux Ch. and Versmold H., *Physica A* to be published.
- [41] Clark N.A., Hurd A.J. and Ackerson B.J., *Nature* **281** (1979) 57–60.
- [42] Lindsay H.M. and Chaikin P.M., *J. Chem. Phys.* **76** (1982) 3774–3781.
- [43] Okubo T., *Colloid Polym. Sci.* **271** (1993) 873–883.
- [44] Pusey P.N., van Megen W., Bartlett P., Ackerson B.J., Rarity J.G. and Underwood S.M., *Phys. Rev. Lett.* **63** (1989) 25.
- [45] Sanders J.V., *Acta Cryst. A* **24** (1968) 427–433.
- [46] Laun H.M., Bung R., Hess S., Loose W., Hess O., Hahn K., Hädicke E., Hingmann R., Schmidt F. and Lindner P., *J. Rheol.* **36** (1992) 743–787.
- [47] Versmold H., *Phys. Rev. Lett.* **75** (1995) 763–766.
- [48] Guinier A., X-ray Diffraction (Freeman, London, 1963).
- [49] Welberry T.R. and Galbraith R., *J. Appl. Cryst.* **6** (1973) 87–96.
- [50] Katchalsky A., Alexandrowicz O. and Koden O., Chemical physics of ionic solutions, B.E. Conway and R.G. Barradas, Eds. (Wiley, 1966) p. 295.
- [51] Bell G.M. and Dunning A.J., *Trans. Faraday Soc.* **66** (1970) 500.
- [52] Belloni L., Thèse de l'université P.M. Curie Paris VI (1982) pp. 21–34.
- [53] Hansen J.P. and McDonald I.A., Theory of simple liquids (Academic Press, New-York 1986).
- [54] Verwey E.J.W. and Overbeek J.Th.G., Theory of the Stability of Lyophobic Colloids (Elsevier, Amsterdam, 1948).
- [55] Robbins M.O., Kremer K. and Grest G.G., *J. Chem. Phys.* **88** (1988) 3286.
- [56] Hone D., Alexander S., Chaikin P.M. and Pincus P., *J. Chem. Phys.* **79** (1983) 1474–1478.
- [57] Shih W.Y., Aksay I.A. and Kikuchi R., *J. Chem. Phys.* **86** (1987) 5127–5132.
- [58] Tejero C.F., Lutsko J.F., Colot J.L. and Baus M., *Phys. Rev. A* **46** (1992) 3373–3379.
- [59] Alexander S., Chaikin P.M., Grant P., Morales G.J., Pincus P. and Hone D., *J. Chem. Phys.* **80** (1984) 11.
- [60] Lindemann F.A., *Z. Phys.* **11** (1910) 609.
- [61] Ohtsuki T., Mitaku S. and Okano K., *Jpn J. Appl. Phys.* **17** (1978) 627.